Chemical Science

ROYAL SOCIETY OF CHEMISTRY

EDGE ARTICLE

View Article Online
View Journal | View Issue

Cite this: *Chem. Sci.*, 2020, **11**, 12103

All publication charges for this article have been paid for by the Royal Society of Chemistry

Received 24th July 2020
Accepted 30th September 2020

DOI: 10.1039/d0sc04044d

rsc.li/chemical-science

Direct synthesis of the organic and Ge free Al containing BOG zeolite (ITQ-47) and its application for transformation of biomass derived molecules†

Qintong Huang,[ab] Ningyue Chen,[a] Lichen Liu,[b] Karen S. Arias,[b] Sara Iborra,[b] Xianfeng Yi,[c] Chao Ma,[d] Weichi Liang,[a] Anmin Zheng,[c] Chuanqi Zhang,[a] Jibo Hu,[a] Zilin Cai,[a] Yi Liu,[e] Jiuxing Jiang *[a] and Avelino Corma *[bf]

Aluminosilicate boggsite (Si/Al-BOG) has been hydrothermally synthesized without adding organic structure-directing agents (OSDAs) in the synthesis gel using the borosilicogermanium ITQ-47 (Si/B-ITQ-47) zeolite as seeds. The introduction of the costly and environmentally less benign phosphazene organic structure-directing agent is not required to grow the zeolite. Physicochemical characterization experiments show that Si/Al-BOG has good crystallinity, high surface area, tetrahedral Al^{3+} species, and acid sites. In order to test the catalytic performance of the zeolite, the synthesis of L,L-lactide from L-lactic acid was performed. Si/Al-BOG exhibits 88.2% conversion of L-lactic acid and 83.8% L,L-lactide selectivity, which are better than those of other zeolites studied up to now.

Introduction

Zeolites and zeotypes are the most successful molecular sieve inorganic materials. In this group of microporous materials, aluminosilicates offer many advantages over phosphates, germanates and other substituted silicate zeolite subgroups.[1] They offer excellent thermal stability, strong acid sites and exchangeable extra-framework cations that enable applications as catalysts, detergents and gas separation materials. Thus, it is highly desired to directly prepare the aluminosilicate counterparts of emerging new zeolites. Currently, among the 252 zeolites accepted by the International Zeolite Association (IZA), there are about 115, which can be synthesized as aluminosilicates by direct hydrothermal synthesis.[2] The rest are borosilicates,[3] gallosilicates,[4] zincosilicate[5] and germanosilicate[6] that could only be transformed into aluminosilicates by post-synthesis treatments,[7] *i.e.*, aluminum reinsertion. Here, we provide an alternative method to synthesize the structurally very interesting and technologically promising zeolite boggsite (ITQ-47), directly as an aluminosilicate instead of the reported silicoborogermanate, without adding the expensive organic structure-directing agents (OSDAs) in the synthesis gel.

Organotemplate-free seed-directed synthesis is regarded as a "green route" for synthesizing zeolites because this synthesis approach is economically and environmentally benign.[8] For instance, Beta(BEA),[9] RUB-13(RTH),[10] ECR-1(EON),[11] Levyne (LEV),[12] ZJM-2 (FER),[13] ZJM-4 (TON),[14] ZJM-6 (MTT),[15] ZSM-34 (OFF-ERI),[16] ZSM-12 (MTW),[17] heulandite (HEU),[12b] UZM-4 (BPH),[18] Mazzite (MAZ),[19] MCM-68 (MSE),[20] MCM-22 (MWW),[21] NU-87 (NES),[22] SUZ-4 (SZR),[23] CIT-1 (CON),[24] SSZ-48 (SFE),[25] VPI-8(VET),[26] and EMC-2(EMT)[27] have been successfully synthesized by this route. However, all the above-mentioned zeolite syntheses use seeds and gels with the same chemical compositions, *i.e.*, Si/Al seed *vs.* Si/Al gel,[9a,11a,12–23,28] Si/B seed *vs.* Si/B gel,[10,24,25] and Si/Zn seed *vs.* Si/Zn gel.[26] Notably, Luo[25] and Yokoi[10] have attempted to synthesize Si/Al-SSZ-48 and Si/Al-RUB-13 through the partial substitution of B with Al in the borosilicate gel, using Si/B-SSZ-48 and Si/B-SSZ-13 as seeds respectively. Unfortunately, the complete substitution attempts failed, and the issue remains unsolved. Here, we present the possibility to grow the Ge free aluminosilicate boggsite starting with the boron germanosilicate form of boggsite (ITQ-47) as a seed and an aluminosilicate synthesis gel. Moreover, we could avoid the use of any organic template by this approach. This is particularly interesting because boggsite has been only

[a]MOE Key Laboratory of Bioinorganic and Synthetic Chemistry, School of Chemistry, Sun Yat-sen University, Guangzhou, 510275, P. R. China. E-mail: jiangjiux@mail.sysu.edu.cn

[b]Instituto de Tecnología Química, Universitat Politècnica de València-Consejo Superior de Investigaciones Científicas, Avenida de los Naranjos s/n, 46022 Valencia, Spain. E-mail: acorma@itq.upv.es

[c]State Key Laboratory of Magnetic Resonance and Atomic and Molecular Physics, National Center for Magnetic Resonance in Wuhan, Wuhan Institute of Physics and Mathematics, Innovation Academy for Precision Measurement Science and Technology, Chinese Academy of Sciences, Wuhan 430071, P. R. China

[d]Zhang Dayu School of Chemistry, Dalian University of Technology, Dalian 116024, Liaoning, China

[e]ZhongShan AKDM Biological Technology Co., Ltd., Zhongshan, 528400, P. R. China

[f]School of Materials Science and Engineering, Zhengzhou University, Zhengzhou, Henan 450001, P. R. China

† Electronic supplementary information (ESI) available. See DOI: 10.1039/d0sc04044d

synthesized in the presence of a very expensive and less environmentally friendly OSDA.

Boggsite is a natural rare aluminosilicate mineral zeolite that possesses intersecting 10-ring (5.1–5.2 Å) and 12-ring (7.2–7.4 Å) channels open to the external surface. The unique pore architecture and aluminosilicate composition endow Boggsite with potential applications in shape-selective acid catalysis. However, as mentioned before, boggsite zeolite mineral is extremely rare, and only small quantities have been found in North America and Antarctica.[29] Recently, Corma and coworkers[30] successfully synthesized the BOG zeolite as borosilicogermanium (Si/B-ITQ-47) by employing a phosphazene OSDA. Unfortunately, Si/B-ITQ-47 presents the following limitations: (a) the phosphazene OSDA and germanium oxide are necessary, environmentally unfriendly and very expensive even for laboratory synthesis, (b) the phosphate residue after calcination has to be necessarily removed to avoid the blocking of the channels, and (c) tetrahedral aluminum sites can only be created by Al reinsertion after washing out boron atoms (Scheme 1a). Here, we will demonstrate the successful direct hydrothermal synthesis of the aluminosilicate form of the BOG zeolite by seed-directed synthesis that can help to overcome the limitations mentioned above. Then, the direct synthesis of the aluminosilicate BOG-type zeolite (Si/Al-BOG) could be achieved with a moderate Si/Al ratio of 9.1 without adding any OSDA to an aluminosilicate synthesis gel, by using Si/B-ITQ-47 (calcined or uncalcined) as the seed. The Si/Al-BOG shows high adsorption ability and high acidity after ammonium exchange/calcination. Besides, the Si/Al-BOG crystals from the synthesis can be used as seeds for a second synthesis Scheme 1.

Experiments

Synthesis of the ITQ-47 seeds

Firstly, Si/B-ITQ-47 seeds were prepared with the gel molar ratio: 0.0235 SiO_2 (TEOS) : 0.0016 GeO_2 : 0.001 H_3BO_3 : 0.010 P1-phosphazene, $H_2O/(SiO_2 + GeO_2) = 10$, and ITQ-47 (1) seed crystals (5 wt% based on the total silica amount).[30] This gel was transferred to a Teflon lined stainless-steel autoclave and heated at 150 °C at its autogenous pressure under tumbling for 25 days. The as-synthesized Si/B-ITQ-47 zeolite was recovered by filtration and dried at 100 °C. The calcined Si/B-ITQ-47 (Si/B-ITQ-47-cal) was obtained by calcining Si/B-ITQ-47 in air at 550 °C to degradate the OSDA located inside of the pores.

Synthesis of the Si/Al-BOG zeolite

The Si/Al-BOG zeolite was then hydrothermally synthesized from synthesis gels with a molar composition of SiO_2 : (0.25–

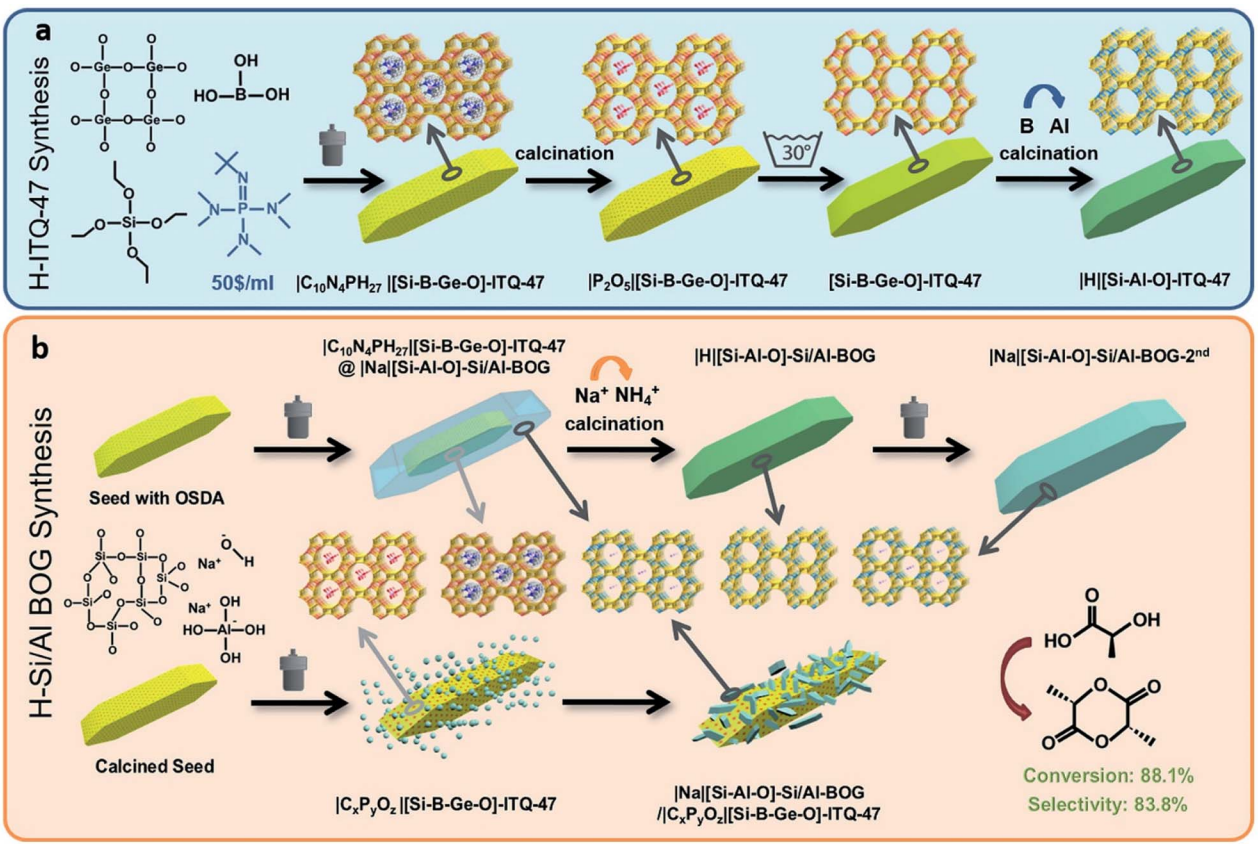

Scheme 1 The comparison between the two methods to prepare an aluminosilicate from zeolite BOG with strong acid sites. (a) Post-synthesis of ITQ-47; (b) seed-directed Si/Al functionalization (note: "autoclave" represents hydrothermal synthesis, "B → Al" indicates post-synthesis treatment of the Si/B-ITQ-47-cal to obtain exchanged Al-ITQ-47, "$Na^+ \rightarrow NH_4^+$" indicates ammonium exchange of zeolites, "@" means the core–shell growth and "/" means the secondary nucleation growth. The chemical formulae are determined by ICP and elemental analysis).

0.28) Na_2O : (0.012–0.020) Al_2O_3 : 20 H_2O and adding 5 wt% of the as-synthesized ITQ-47 or 6.7 wt% of the calcined ITQ-47 synthesized above (based on the total silica amount), as fresh or after calcination to remove the template, respectively. After stirring at room temperature, the mixtures were transferred into autoclaves for crystallization at 125 °C for 14 days. Then, the samples washed with deionized water were dried at 100 °C, and named Si/Al-BOG (when synthesized with the OSDA containing seeds), and S_{cal}-Si/Al-BOG (when synthesized with the OSDA free calcined seeds). The acidic form of the Si/Al-BOG (H-Si/Al-BOG) zeolite was obtained by ion-exchange with 1 M NH_4NO_3 aqueous solution at 50 °C for 5 h (1 g of Si/Al-BOG zeolite in 50 mL of solution), followed by calcination at 550 °C for 5 h. When the Si/Al-BOG zeolite was used as seeds for a second synthesis, the sample denoted as Si/Al-BOG-2^{nd} was obtained under similar synthesis conditions. For comparison, the Al-ITQ-47 was prepared by a B–Al exchange process. The chemical composition of Si/B-ITQ-47, Si/B-ITQ-47-cal, exchanged Al-ITQ-47, Si/Al-BOG, H-Si/Al-BOG, S_{cal}-Si/Al-BOG, and Si/Al-BOG-2^{nd}, is given in Tables S1 and S2.† Detailed information on zeolite synthesis can be found in the ESI.†[31] The yields of Si/Al-BOG, S_{cal}-Si/Al-BOG, and Si/Al-BOG-2^{nd} are 30.3%, 26.6% and 29.5% calculated by using the formula:

$$\text{Yield} = (W_{\text{product}} - W_{\text{seed}} - W_{\text{amorphous}})/(W_{SiO_2} + W_{Al_2O_3})$$

Results and discussion

The powder XRD patterns of the Si/B-ITQ-47 seed (Fig. 1b), as-synthesized Si/Al-BOG (Fig. 1c), NH_4^+ exchanged and calcined acidic form of the H-Si/Al-BOG zeolite (Fig. 1d), re-seeded product Si/Al-BOG-2^{nd} (Fig. 1e), Si/B-ITQ-47-cal seed (Fig. 1f), and direct synthesis with calcined seed S_{cal}-Si/Al-BOG (Fig. 1g) samples are well fitted with simulated BOG XRD (Fig. 1a). However, the slightly broadened XRD peaks around 25° in Si/Al-BOG-2^{nd} and S_{cal}-Si/Al-BOG samples imply the presence of an amorphous impurity (Fig. S1†).

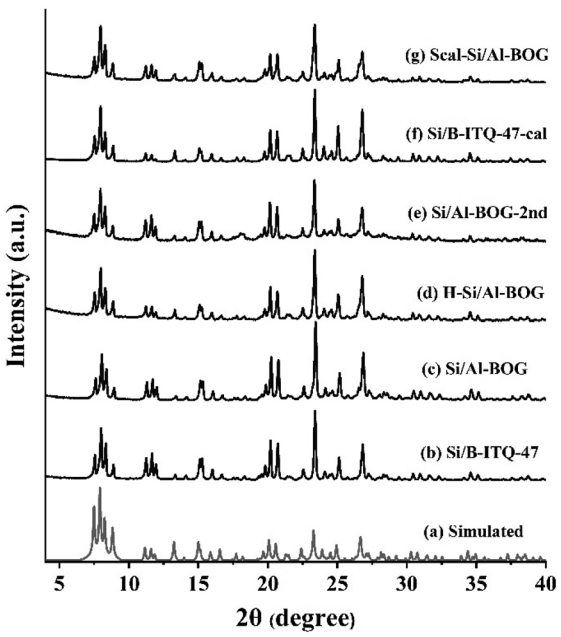

Fig. 1 Powder XRD patterns of (a) BOG simulated, (b) Si/B-ITQ-47, (c) Si/Al-BOG, (d) H-Si/Al-BOG, (e) Si/Al-BOG-2^{nd}, (f) Si/B-ITQ-47-cal, and (g) S_{cal}-Si/Al-BOG.

The elemental analysis results of Si/B-ITQ-47, Si/B-ITQ-47-cal, exchanged Al-ITQ-47, Si/Al-BOG, H-Si/Al-BOG, S_{cal}-Si/Al-BOG and Si/Al-BOG-2^{nd} are summarized in Tables S1 and S2.† ICP analysis of Si/Al-BOG, S_{cal}-Si/Al-BOG, and Si/Al-BOG-2^{nd} shows that Si/Al ratios are 9.1, 10.9, and 7.8, respectively, which are higher than that of the naturally occurring boggsite mineral (Si/Al = 4.2). Compared to the total 12.63% of C, N, and P weight percentage coming from the OSDA in the Si/B-ITQ-47, Si/Al-BOG and Si/Al-BOG-2^{nd} contain only 5.15% and 2.62% phosphazene template of the Si/B-ITQ-47 seed, respectively. Furthermore, the C/P ratio (11.3) and N/P (5.1) ratio for Si/B-ITQ-47 are quite close to the theoretical values (10 and 4, respectively), indicating the structural integrity of the phosphazene molecules, whereas, the C/P = 14.98, N/P = 7.17 for the Si/Al-BOG and C/P = 17.48, N/P = 4.47 for the Si/Al-BOG-2^{nd}, are far from theoretical values implying the partial decomposition of phosphazene during the hydrothermal synthesis. The S_{cal}-Si/Al-BOG sample still contains 0.80% of phosphate and 0.46% carbon species. Nevertheless, it is clear that with the S_{cal}-Si/Al-BOG sample, any structure-directing effect of the potential residual OSDA remaining in the Si/B-ITQ-47-cal seed can be neglected since we could not detect nitrogen in the final sample. As is known, the phosphate species (in this case coming from the calcined seeds), usually remains in the channel of the zeolite. The sodium content of H-Si/Al-BOG is 0.01% that is about the experimental error of ICP analysis indicating the completeness of NH_4^+ ion exchange. Si/Al-BOG, S_{cal}-Si/Al-BOG and Si/Al-BOG-2^{nd} show a similar weight loss, *ca.* 10% below 200 °C that could be attributed to adsorbed and coordinated water. The 6.0% and 2.7% weight loss of Si/Al-BOG and Si/Al-BOG-2^{nd} between 200 and 600 °C roughly correspond to the removable carbon and nitrogen content of phosphazene coming from the seed, *i.e.*, 4.6% and 2.4% respectively, whereas, the S_{cal}-Si/Al-BOG shows a minimal (1.3%) weight loss between 200 and 600 °C (Fig. S2†). Scanning electron microscope (SEM) images of Si/B-ITQ-47 (Fig. 2a and S3a†) show a layer stacking morphology with relatively uniform crystal size distribution, displaying a length of 3–7 μm and a width of 0.5–2.5 μm, whereas, the Si/Al-BOG crystallites (Fig. 2b and S3c†) exhibit a randomly intergrown spindle-like morphology, *i.e.*, a mixture of large crystallites (3–14 μm in length and ~2 μm in width) and small crystallites (0.5–2 μm in length and ~0.5 μm in width). The particle size distribution shows two peaks centered at 1.5 μm and 5.5 μm (see particle size distribution in Fig. S3b and d†). Note that the amount of small crystallites corresponds to 91% of the total. The Scanning Transmission Electron Microscopy-Energy Dispersive spectroscopy (STEM-EDS) mapping of the small Si/Al-BOG zeolite crystallite confirms the presence of Si, Al, P, Ge and B atoms in the Si/Al-BOG sample (Fig. 2d–i). Notably, there is a clear boundary of element distribution, which delimits the

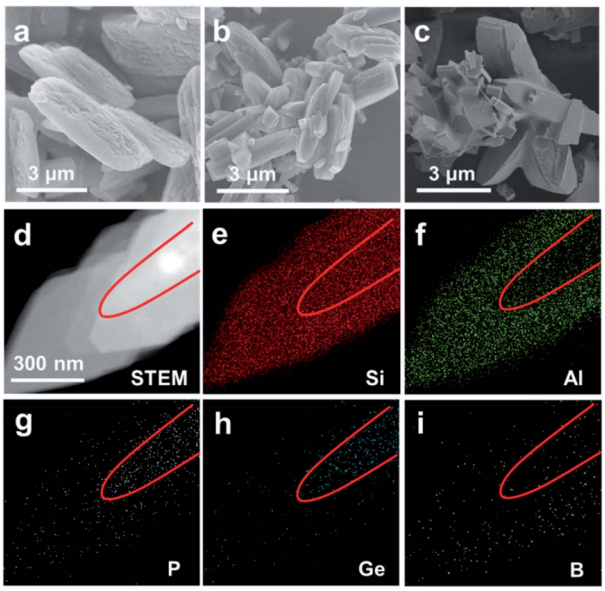

Fig. 2 SEM images of (a) Si/B-ITQ-47 seed, (b) Si/Al-BOG, and (c) Si/Al-BOG-2nd. (d) STEM image of a selected crystal of Si/Al-BOG; TEM element mapping of (e) Si, (f) Al, (g) P, (h) Ge, and (i) B corresponding to STEM images.

crystal into two parts, the inner part is P and Ge rich (coming from Si/B-ITQ-47 seeds), whereas the outer part is aluminum-rich (coming from Si/Al-BOG). Interestingly, B atoms do not follow the trend; they redistribute among the core–shell structure. The detailed mechanism is under investigation. Furthermore, EDS line-scan cross-section analysis of a single crystallite (Fig. S4†) also indicates that the Ge-containing nucleus is surrounded by the aluminosilicate shell. Taking into account the fact that these small crystallites in the Si/Al-BOG sample are clearly much smaller than the starting Si/B-ITQ-47 seeds, we speculate that a large part of the parent Si/B-ITQ-47 should be transformed into smaller entities/nucleus containing B, P, and Ge during the hydrothermal treatment. Those nucleuses could further result in the core–shell growth[32] to form the small final crystals during the crystallization process, following the mechanism illustrated in Scheme 1b. Nevertheless, high-resolution TEM shows an excellent crystallinity of Si/Al-BOG (Fig. S5†). The crystallographic axis of Si/Al-BOG was found by electronic diffraction (Fig. S6†).

The Si/Al-BOG sample prepared with the Si/B-ITQ-47-cal seed (S_{cal}-Si/Al-BOG sample) also shows a bi-modal morphology. As can be seen in Fig. S3e,† a mixture of large (3–8 μm in length and ~1.5 μm in width) and small crystallites (0.5–2 μm in length and 0.2–0.5 μm in width) is observed (Fig. S3f†). The large crystallites show similar size and morphology to the parent Si/B-ITQ-47-cal while the vast majority of the crystallites also exist as much smaller particles. Furthermore, STEM-EDS mapping observations on several typical areas of this sample fail to detect the core–shell structure on the small crystallites (Fig. S7†). Therefore, it is speculated that the dissolution–recrystallization mechanism (secondary nucleation) plays a predominant role during the formation of S_{cal}-Si/Al-BOG (Scheme 1b). Such a difference could be caused by the faster dissolution of the Si/B-ITQ-47-cal seed since the bulky OSDA molecules were removed by calcination, which further facilitated the formation of the nucleus. If so, it can be expected that the use of Si/Al-BOG for a second seed-mediated growth of the BOG zeolite will exhibit a similar product morphology since no bulky OSDA is present in the Si/Al-BOG sample. Indeed, as can be seen in the morphological characterization of the Si/Al-BOG-2nd sample (Fig. 2c and S8†), similar behaviors are witnessed as for the S_{cal}-Si/Al-BOG, indicating that the secondary nucleation mechanism is also the main pathway of crystallization.

Fig. S9† shows the N_2 sorption isotherms of the Si/B-ITQ-47-cal and sodium form/acid form of Si/Al-BOG, Si/Al-BOG-2nd and S_{cal}-Si/Al-BOG samples. Si/B-ITQ-47-cal shows a comparable Brunauer–Emmett–Teller (BET) surface area, *i.e.*, 600 $m^2\ g^{-1}$ *vs.* 582 $m^2\ g^{-1}$ and micropore volume, *i.e.*, 0.22 $cm^3\ g^{-1}$ *vs.* 0.22 $cm^3\ g^{-1}$ to those of the Si/B-ITQ-47-cal reported in the literature. The BET surface area and micropore volume for the sodium form of Si/Al-BOG (522 $m^2\ g^{-1}$, 0.20 $cm^3\ g^{-1}$), Si/Al-BOG-2nd (391 $m^2\ g^{-1}$, 0.15 $cm^3\ g^{-1}$), and S_{cal}-Si/Al-BOG (496 $m^2\ g^{-1}$, 0.19 $cm^3\ g^{-1}$) are lower than those of Si/B-ITQ-47-cal, due to the presence of some amorphous material present in the sample as well as the presence of Na^+ in the channels (Table S3†). Without surprise, the acid forms of H-Si/Al-BOG (582 $m^2\ g^{-1}$, 0.22 $cm^3\ g^{-1}$), H-Si/Al-BOG-2nd (458 $m^2\ g^{-1}$, 0.17 $cm^3\ g^{-1}$), and H-S_{cal}-Si/Al-BOG (528 $m^2\ g^{-1}$, 0.20 $cm^3\ g^{-1}$) reveal the extra surface area and pore volume released during the Na^+ removal by ion exchange treatment.

To quantify the amorphous phase inferred by a broad XRD band around 25° in spectra of the S_{cal}-Si/Al-BOG and Si/Al-BOG-2nd, ^{29}Si NMR spectroscopy was carried out and the peaks were deconvoluted (Table S4, Fig. S10†). Firstly, we assign four peaks, *i.e.*, −112, −108, −102, and −98 ppm to Q4, Q3, Q2, and Q1, respectively. And then, the broad differential spectrum peak around −105 ppm automatically appears, that can be attributed to the amorphism.[33] Following the same procedure, S_{cal}-Si/Al-BOG and Si/Al-BOG-2nd are proposed to contain about 18% amorphous phase. Notice that 9% amorphous species is also detected in Si/Al-BOG, though the broad XRD peak around 25° was not clearly shown for this sample (Fig. S1†), and enlarged SEM images of Si/Al-BOG (Fig. S3c†), Si/Al-BOG-2nd (Fig. S6†) and S_{cal}-Si/Al-BOG (Fig. S3e†) present no obvious amorphism. ^{27}Al-MAS-NMR spectroscopy (Fig. S11†) shows an intense resonance peak at 57.8 ppm, which is attributed to tetrahedrally coordinated Al centers.[33,34] Compared with ITQ-47 prepared by aluminum reinsertion, the spectrum of the Si/Al-BOG is 2.8 ppm downfield. The negligible peak around 0 ppm indicates that the extra-framework hexacoordinated Al atoms are mostly avoided in the seed directed synthesis.

The NH_3-TPD profile of H-Si/Al-BOG presents desorption peaks around 146 °C, 401 °C, and 550 °C, corresponding to NH_3 adsorbed on acid sites with different heats of adsorption (Fig. S12†).[35] Further infrared spectra of pyridine absorbed H-Si/Al-BOG at desorption temperatures of 150 °C, 250 °C and 350 °C in a vacuum show clear peaks at 1546 cm^{-1} and 1454 cm^{-1}, which can be associated with Brønsted and Lewis acid sites respectively. This indicates that strong Brønsted (≡Al–OH–Si≡) sites and Lewis acid sites are present in the H-Si/Al-BOG sample (Fig. S13†). We quantify the acidity of H-Si/Al-BOG by the catalyst poisoning method using pyridine as the probe molecule.[36] The intercept of *x*-axis of the plot

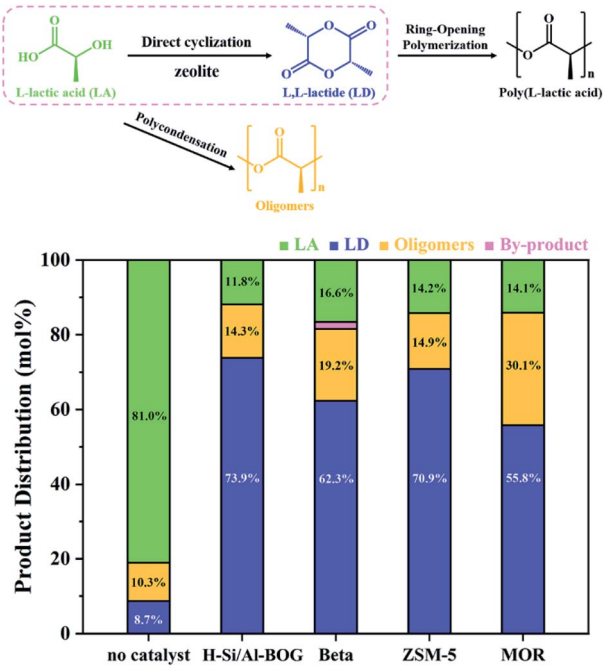

Fig. 3 The product distribution of L-lactic acid to L,L-lactide over the selected zeolites. LA (lactic acid); LD (L,L-lactide).

between L,L-lactide yield (%) and the amount of pyridine added (Fig. S14†), provides the concentration of the acidic sites, which is found to be 251.3 μmol g^{-1}.

Zeolites have demonstrated shape selectivity for the synthesis of the optically pure L,L-lactide from L-lactic acid.[37] The BOG structure has interconnected 12- and 10-ring channels and Brønsted acid sites, which is ideal for the direct conversion of concentrated aqueous L-lactic acid to L,L-lactide. Fig. 3 shows the comparison of the catalytic performance of H-form of the Si/Al-BOG zeolite with several commercially available zeolites at a reaction time of 4 h at 144 °C in *o*-xylene. The results in Fig. 3 show that the acidic form of the H-Si/Al-BOG zeolite exhibits higher total conversion and higher yield and selectivity for L,L-lactide than the commercial ZSM-5 zeolite (CBV3024E, Si/Al = 15), and substantially higher than Beta (CP811, Si/Al = 12.5) and MOR zeolites (CBV20A, Si/Al = 10). Thus, the aluminosilicate form of BOG shows potential as a zeolite catalyst for the transformation of biomass-derived platform molecules. Meanwhile, the recycling performance in Fig. S15† shows that the catalyst retained most of the catalytic activity after five cycles of reaction. Fig. S16† shows that the catalytic performance of H-S_{cal}-Si/Al-BOG is comparable with H-Si/Al-BOG. Fig. S17† provides a demonstration of quantification of the products using ^{1}H-NMR. The pore structure of the boggsite formed by 12 × 10-ring pore channels, together with the improved synthesis method opens new opportunities for the use of aluminosilicate BOG in catalysis.

Conclusions

In conclusion, we have shown in this work the possibility to directly synthesize the aluminosilicate form of boggsite in the absence of OSDAs. This result is not only of fundamental interest, but it opens practical opportunities for industrial application of this exciting zeolite structure that combines large and medium pores in the structure. When compared with conventional H-beta and H-ZSM-5 zeolite catalysts, the acidic form of H-Si/Al-BOG exhibits higher conversion of L-lactic acid and higher selectivity for L,L-lactide.

Conflicts of interest

There are no conflicts to declare.

Acknowledgements

This work was supported by the National Natural Science Foundation of China 21971259 and 91645112, The Natural Science Foundation of Hubei Province of China (2014CFA043), and the Key Research Program of Frontier Sciences, CAS (No. QYZDB-SSW-SLH026). The European Union is also acknowledged by ERC-AdG-2014-671093 SynCatMatch, and the Spanish Government through "Severo Ochoa" (SEV-2016-0683, MINECO). Q. H. acknowledges the International Program Fund for doctoral students, Sun Yat-sen University, for scholarships in Spain.

Notes and references

1 C. S. Cundy and P. A. Cox, *Chem. Rev.*, 2003, **103**, 663–702.
2 C. Baerlocher and L. B. McCusker, *Database of Zeolite Structures*, http://www.iza-structure.org/databases/, accessed June 8, 2018.
3 (*a*) R. F. Lobo, M. Pan, I. Chan, R. C. Medrud, S. I. Zones, P. A. Crozier and M. E. Davis, *J. Phys. Chem.*, 1994, **98**, 12040–12052; (*b*) R. F. Lobo, M. Pan, I. Chan, H. X. Li, R. C. Medrud, S. I. Zones, P. A. Crozier and M. E. Davis, *Science*, 1993, **262**, 1543–1546; (*c*) B. Marler, A. Grünewald-Luke and H. Gies, *Zeolites*, 1995, **15**, 388–399; (*d*) A. Burton, R. J. Darton, M. E. Davis, S. J. Hwang, R. E. Morris, I. Ogino and S. I. Zones, *J. Phys. Chem. B*, 2006, **110**, 5273–5278; (*e*) F. L. Raul and E. D. Mark, *J. Am. Chem. Soc.*, 1995, **117**, 3766–3779; (*f*) W. Paul, N. Yumi, S. L. Greg, E. D. Mark, E. Saleh, C. M. Ronald and S. I. Zones, *J. Am. Chem. Soc.*, 2000, **122**, 263–273; (*g*) S. Vortmann, B. Marler, H. Gies and P. Daniels, *Microporous Mater.*, 1995, **4**, 111–121; (*h*) P. Wagner, O. Terasaki, S. Ritsch, J. G. Nery, S. I. Zones, M. E. Davis and K. Hiraga, *J. Phys. Chem. B*, 1999, **103**, 8245–8250; (*i*) A. Burton, S. Elomari, R. C. Medrud, I. Y. Chan, C.-Y. Chen, L. M. Bull and E. S. Vittoratos, *J. Am. Chem. Soc.*, 2003, **125**, 1633–1642; (*j*) A. Burton, S. Elomari, C.-Y. Chen, R. C. Medrud, I. Y. Chan, L. M. Bull, C. Kibby, T. V. Harris, S. I. Zones and E. S. Vittoratos, *Chem.–Eur. J.*, 2003, **9**, 5737–5748; (*k*) S. Elomari, A. Burton, R. C. Medrud and R. Grosse-Kunstleve, *Microporous Mesoporous Mater.*, 2009, **118**, 325–333; (*l*) S. Elomari, A. W. Burton, K. Ong, A. R. Pradhan and I. Y. Chan, *Chem. Mater.*, 2007, **19**, 5485–5492; (*m*) A. Burton and S. Elomari, *Chem. Commun.*, 2004, 2618–2619, DOI: 10.1039/B410010G; (*n*) D. Xie,

L. McCusker and C. Baerlocher, *J. Am. Chem. Soc.*, 2011, **133**, 20604–20610.

4 K. G. Strohmaier and D. E. W. Vaughan, *J. Am. Chem. Soc.*, 2003, **125**, 16035–16039.

5 (*a*) C. C. Freyhardt, R. F. Lobo, S. Khodabandeh, J. E. Lewis, M. Tsapatsis, M. Yoshikawa, M. A. Camblor, M. Pan, M. M. Helmkamp, S. I. Zones and M. E. Davis, *J. Am. Chem. Soc.*, 1996, **118**, 7299–7310; (*b*) M. E. Davis and J. C. McKeen, *J. Phys. Chem. C*, 2009, **113**, 9870–9877.

6 (*a*) J. Jiang, J. Yu and A. Corma, *Angew. Chem., Int. Ed.*, 2010, **49**, 3120–3145; (*b*) J. Jiang, J. L. Jorda, M. J. Diaz-Cabanas, J. Yu and A. Corma, *Angew. Chem., Int. Ed.*, 2010, **49**, 4986–4988; (*c*) J. Jiang, J. L. Jorda, J. Yu, L. A. Baumes, E. Mugnaioli, M. J. Diaz-Cabanas, U. Kolb and A. Corma, *Science*, 2011, **333**, 1131–1134; (*d*) J. Jiang, Y. Yun, X. Zou, J. L. Jorda and A. Corma, *Chem. Sci.*, 2015, **6**, 480–485; (*e*) C. Zhang, E. Kapaca, J. Li, Y. Liu, X. Yi, A. Zheng, X. Zou, J. Jiang and J. Yu, *Angew. Chem., Int. Ed.*, 2018, **57**, 6486–6490; (*f*) J. Y. Li, A. Corma and J. H. Yu, *Chem. Soc. Rev.*, 2015, **44**, 7112–7127; (*g*) Y. Li and J. Yu, *Chem. Rev.*, 2014, **114**, 7268–7316.

7 (*a*) C. Y. Chen and S. I. Zones, in *Zeolite and Catalysis: Synthesis, Reaction and Application*, ed. A. C. Jiri Cejka and S. Zones, Wiley-VCH Verlag GmbH & Co. KGaA, Weinheim, 2010, ch. 6, vol. 1, pp. 155–164; (*b*) V. Valtchev, G. Majano, S. Mintova and J. Perez-Ramirez, *Chem. Soc. Rev.*, 2013, **42**, 263–290; (*c*) S. I. Zones, A. Benin, S.-J. Hwang, D. Xie, S. Elomari and M.-F. Hsieh, *J. Am. Chem. Soc.*, 2014, **136**, 1462–1471; (*d*) F. F. Gao, M. Jaber, K. Bozhilov, A. Vicente, C. Fernandez and V. Valtchev, *J. Am. Chem. Soc.*, 2009, **131**, 16580–16586.

8 (*a*) X. J. Meng and F. S. Xiao, *Chem. Rev.*, 2014, **114**, 1521–1543; (*b*) K. Iyoki, K. Itabashi and T. Okubo, *Microporous Mesoporous Mater.*, 2014, **189**, 22–30.

9 (*a*) B. Xie, J. W. Song, L. M. Ren, Y. Y. Ji, J. X. Li and F. S. Xiao, *Chem. Mater.*, 2008, **20**, 4533–4535; (*b*) H. Y. Zhang, B. Xie, X. J. Meng, U. Muller, B. Yilmaz, M. Feyen, S. Maurer, H. Gies, T. Tatsumi, X. H. Bao, W. P. Zhang, D. De Vos and F. S. Xiao, *Microporous Mesoporous Mater.*, 2013, **180**, 123–129; (*c*) Y. M. Liao, S. X. Pan, C. Q. Bian, X. J. Meng and F. S. Xiao, *J. Mater. Chem. A*, 2015, **3**, 5811–5814.

10 T. Yokoi, M. Yoshioka, H. Imai and T. Tatsumi, *Angew. Chem., Int. Ed.*, 2009, **48**, 9884–9887.

11 (*a*) J. W. Song, L. Dai, Y. Y. Ji and F. S. Xiao, *Chem. Mater.*, 2006, **18**, 2775–2777; (*b*) L.-M. Ren, L.-F. Zhu, H. Ding, C.-G. Yang, X.-J. Meng and F.-S. Xiao, *Chem. J. Chin. Univ.*, 2011, **32**, 662–666.

12 (*a*) H. Zhang, C. Yang, L. Zhu, X. Meng, B. Yilmaz, U. Mueller, M. Feyen and F.-S. Xiao, *Microporous Mesoporous Mater.*, 2012, **155**, 1–7; (*b*) B. Xie, H. Y. Zhang, C. G. Yang, S. Y. Liu, L. M. Ren, L. Zhang, X. J. Meng, B. Yilmaz, U. Muller and F. S. Xiao, *Chem. Commun.*, 2011, **47**, 3945–3947.

13 H. Y. Zhang, Q. Guo, L. M. Ren, C. G. Yang, L. F. Zhu, X. J. Meng, C. Li and F. S. Xiao, *J. Mater. Chem.*, 2011, **21**, 9494–9497.

14 Y. Q. Wang, X. Wang, Q. M. Wu, X. J. Meng, Y. Y. Jin, X. Z. Zhou and F. S. Xiao, *Catal. Today*, 2014, **226**, 103–108.

15 Q. M. Wu, X. Wang, X. J. Meng, C. G. Yang, Y. Liu, Y. Y. Jin, Q. Yang and F. S. Xiao, *Microporous Mesoporous Mater.*, 2014, **186**, 106–112.

16 (*a*) L. Zhang, C. G. Yang, X. J. Meng, B. Xie, L. Wang, L. M. Ren, S. J. Ma and F. S. Xiao, *Chem. Mater.*, 2010, **22**, 3099–3107; (*b*) C. G. Yang, L. M. Ren, H. Y. Zhang, L. F. Zhu, L. Wang, X. J. Meng and F. S. Xiao, *J. Mater. Chem.*, 2012, **22**, 12238–12245.

17 (*a*) K. Iyoki, Y. Kamimura, K. Itabashi, A. Shimojima and T. Okubo, *Chem. Lett.*, 2010, **39**, 730–731; (*b*) Y. Kamimura, K. Iyoki, S. P. Elangovan, K. Itabashi, A. Shimojima and T. Okubo, *Microporous Mesoporous Mater.*, 2012, **163**, 282–290.

18 T. Moteki and T. Okubo, *Chem. Mater.*, 2013, **25**, 2603–2609.

19 A. Ogawa, K. Iyoki, Y. Kamimura, S. P. Elangovan, K. Itabashi and T. Okubo, *Microporous Mesoporous Mater.*, 2014, **186**, 21–28.

20 Y. Kubota, K. Itabashi, S. Inagaki, Y. Nishita, R. Komatsu, Y. Tsuboi, S. Shinoda and T. Okubo, *Chem. Mater.*, 2014, **26**, 1250–1259.

21 Y. Kamimura, K. Itabashi, Y. Kon, A. Endo and T. Okubo, *Chem.–Asian J.*, 2017, **12**, 530–542.

22 K. Iyoki, M. Takase, K. Itabashi, K. Muraoka, W. Chaikittisilp and T. Okubo, *Microporous Mesoporous Mater.*, 2015, **215**, 191–198.

23 H. Zhou, Y. Wu, W. Zhang and J. Wang, *Chin. J. Chem. Eng.*, 2014, **22**, 120–126.

24 S. Sogukkanli, K. Iyoki, S. P. Elangovan, K. Itabashi and T. Okubo, *Chem. Lett.*, 2017, **46**, 1419–1421.

25 Y. Luo, Z. Wang, J. Sun, Y. Wang, S. Jin, B. Zhang, H. Sun and W. Yang, *Chem.–Eur. J.*, 2018, **24**, 306.

26 K. Iyoki, K. Itabashi, W. Chaikittisilp, S. P. Elangovan, T. Wakihara, S. Kohara and T. Okubo, *Chem. Mater.*, 2014, **26**, 1957–1966.

27 E.-P. Ng, D. Chateigner, T. Bein, V. Valtchev and S. Mintova, *Science*, 2012, **335**, 70–73.

28 Y. Kamimura, K. Itabashi and T. Okubo, *Microporous Mesoporous Mater.*, 2012, **147**, 149–156.

29 J. J. Pluth and J. V. Smith, *Am. Mineral.*, 1990, **75**, 501–507.

30 R. Simancas, D. Dari, N. Velamazán, M. Navarro, A. Cantín, J. Jordá, G. Sastre, A. Corma and F. Rey, *Science*, 2010, **330**, 1219–1222.

31 J. Jiang, Q. Huang, C. Zhang, C. Teng and J. Qiu, Aluminosilicate zeolite with BOG structure and its preparation method, CN Pat., CN106976889B, 2017.

32 (*a*) A. G. Arian Ghorbanpour, L. C. Grabow, S. P. Crossley and J. D. Rimer, *ACS Nano*, 2015, **9**, 4006–4016; (*b*) Y. Bouizi, L. Rouleau and V. P. Valtchev, *Microporous Mesoporous Mater.*, 2006, **91**, 70–77.

33 J. Pérez-Pariente, J. Sanz, V. Fornés and A. Corma, *J. Catal.*, 1990, **124**, 217–223.

34 P. Lentz, J. B. Nagy, L. Delevoye, Y. Dumazy, C. Fernandez, J.-P. Amoureux, C. V. Tuoto and A. Nastro, *Colloids Surf., A*, 1999, **158**, 13–20.

35 M. Boronat and A. Corma, *ACS Catal.*, 2019, **9**, 1539–1548.

36 A. Maity, S. Chaudhari, J. J. Titman and V. Polshettiwar, *Nat. Commun.*, 2020, **11**, 3828.

37 M. Dusselier, P. V. Wouwe, A. Dewaele, P. A. Jacobs and B. F. Sels, *Science*, 2015, **349**, 78–80.

